RSC Advances

PAPER

View Article Online
View Journal | View Issue

Cite this: *RSC Adv.*, 2017, **7**, 13347

Highly dispersed Ag/TiO_2 *via* adsorptive self-assembly for bactericidal application

Chongjiang Cao,*[a] Jingcheng Huang,[b] Li Li,[a] Chanjuan Zhao[a] and Jianfeng Yao[c]

Received 18th January 2017
Accepted 19th February 2017

DOI: 10.1039/c7ra00758b

rsc.li/rsc-advances

The strong electrostatic adsorption (SEA) technique was used for the preparation of Ag/TiO_2 by driving the Ag precursor onto the TiO_2 surface. The prepared material was characterized using nitrogen adsorption–desorption techniques, X-ray diffraction, scanning transmission electron microscopy, X-ray photoelectron spectroscopy and inductively-coupled plasma. The results demonstrated that the SEA method could effectively prevent Ag itself from aggregating, and Ag nanoparticles (<2 nm) were formed on the TiO_2 surface with a uniform distribution. To prove the feasibility of the effective SEA method, the bactericidal performance of Ag/TiO_2 particles for antibacterial packaging was evaluated and the results indicated that the highly dispersed Ag on TiO_2 exhibited excellent antimicrobial properties since the particle size and dispersion of Ag nanoparticles have a strong relationship with the inhibition of bacterial growth.

1. Introduction

The antibacterial properties of silver have been widely studied in the literature. Silver ions can lead to denaturation of protein and cell death because of their reaction with nucleophilic amino acid residues in proteins, and attach to sulphydryl, amino, imidazole, phosphate and carboxyl groups of membrane or enzyme proteins.[1–3] Another hypothesis of the antibacterial mechanism is that silver ions are in the catalytic activity center that activates water and oxygen in the air to produce hydroxyl free radicals and active oxygen ions (O^{2-}). Active oxygen ions can destroy the reproductive ability of mould in a short time to induce cell death.[4–6] Such a mechanism does not need any direct contact between antimicrobial agent and bacteria, because the produced active oxygen ions will automatically diffuse from the bulk metal to the surrounding environment. Nanoparticles exhibit completely new and improved properties based on specific characteristics such as size, distribution and morphology in comparison with their bulk counterparts.[7–10] However, it is known that the high surface energy of Ag nanoparticles makes them easily aggregate into big particles, which could deteriorate their unique chemical properties and induce loss of overall performance. To stabilize Ag nanoparticles, an efficient method is to design highly dispersed Ag particles on substrates such as SiO_2, Fe_2O_3, Al_2O_3, and TiO_2.[11–18] Especially, TiO_2 has received considerable attention due to its good stability, environmentally benignity, safety and broad-spectrum antibiosis.[17] Much attention has been focused on combing Ag and TiO_2 to improve antimicrobial activity. Recently, nanocomposite food packages, produced by incorporating nanoparticles of Ag and TiO_2, have been used in several agricultural products, such as mushrooms and strawberries.[18–20] Very recently, it is reported that nano-packaging with Ag/TiO_2 had a quite beneficial antimildew effect on rice storage.[21] Therefore, Ag/TiO_2 nanocomposites show great promise as efficient antibacterials in future.[22–26]

In practical application, both particle size and silver release are two important characteristics for silver-based functional materials. Ag particles of less than 10 nm are expected and they are more toxic to bacteria including *Escherichia coli*.[27,28] However, it is difficult to produce uniform Ag nanoparticles that can strongly anchor on TiO_2 surface by conventional sol–gel and photodeposition methods.[29–31] A simple and rational approach to synthesizing highly dispersed, monometallic catalysts on a wide variety of oxide and carbon supports was developed using the strong electrostatic adsorption (SEA) method.[32–35] The SEA method is based on an electrostatic mechanism[36] in which the hydroxyl groups that populate oxide surfaces become protonated (positively charged) or deprotonated (negatively charged) depending on a characteristic pH value. The particular pH where the hydroxyl groups are neutral is termed the Point of Zero Charge (PZC). According to the theory, the oxides placed in solutions with equilibrium pH values above their PZC would adsorb cations such as silver ammonium ion $[Ag(NH_3)_2]^+$. These electrostatic interactions can be used to control the complex deposition.

In this work, we addressed the use of SEA method for the preparation of Ag-promoted TiO_2 by driving Ag onto TiO_2 phase.

[a]National Engineering Laboratory for Food Storage and Transportation, College of Food Science and Engineering/Collaborative Innovation Center for Modern Grain Circulation and Safety, Nanjing University of Finance & Economics, Nanjing 210023, China. E-mail: ccj33@163.com; Fax: +86 13770625999; Tel: +86 13770625999

[b]Department of Chemistry, Tufts University, Medford, MA 02155, USA

[c]College of Chemical Engineering, Nanjing Forestry University, Nanjing 210037, China

This was achieved by first measuring the PZC of TiO_2 to determine its unique oxide charging parameters. Then the adsorption survey of $[Ag(NH_3)_2]^+$ on TiO_2 at various pH values was conducted. The $[Ag(NH_3)_2]^+$ should strongly adsorb at high pH over high-PZC material such as TiO_2. This information was used to determine the optimal uptake pH for $[Ag(NH_3)_2]^+$ to adsorb onto the supported TiO_2 for Ag/TiO_2 preparation. The antibacterial analysis of Ag/TiO_2 particles was carried out by minimum inhibitory concentration technique.

2. Experimental section

2.1 PZC measurements and adsorption experiments

The two different pure commercial TiO_2 and nano-sized TiO_2 (denoted as TiO_2-N) were obtained from Nanjing Dingbei biological technology Company, China. To determine their PZC, the materials were weighed out to obtain surface loadings of 1000, 10 000 and 50 000 $m^2\ L^{-1}$ for 50 mL of solution. The pH values of each 50 mL deionized water were adjusted in the range of 2–13 by using HCl or NaOH. Then TiO_2 was added to the above pH adjusted solutions and shaked for 1 h. Final pH measurements were obtained using a general combination pH electrode. At sufficiently high surface loadings, the plateau of the pH shift plot corresponds to the PZC of the support.[37] The PZCs of TiO_2 and nano-TiO_2 are 6.9 and 7.1 respectively. Preliminary equilibrium adsorption experiments to study $[Ag(NH_3)_2]^+$ uptake were performed over the pure TiO_2 and TiO_2-N materials. The pH-adjusted $[Ag(NH_3)_2]^+$ (solutions 200 ppm Ag) were contacted with the pure oxides at a surface loading of 500 $m^2\ L^{-1}$, in excess liquid to prevent large shifts in the solution pH due to the oxide,[37] shaken for 1 h, and then ~5 mL of solution was filtered off to analyze Ag concentration using a Perkin-Elmer Inductively Coupled Plasma-Optical Emission Spectrometer (ICP-OES). Ag uptake can be calculated with difference in concentration between the pre- and post-contacted solutions.

2.2 Materials preparation

Ag promoted TiO_2 samples were prepared by SEA as follows: the equilibrium adsorption uptake of $[Ag(NH_3)_2]^+$ onto TiO_2 and TiO_2-N was determined as a function of pH from solutions with a fixed metal concentration (200 ppm Ag). Larger samples (1 g) of catalysts were prepared at the pH of maximum uptake, which corresponds to optimal condition for SEA. Shaken 1 h and then the filtered solids were dried overnight and then irradiated with UV light (100 W mercury lamp from Philips) for 1 h. The samples properties are listed in Table 1.

2.3 Physical characterization

X-ray diffraction (XRD) analysis was performed on a Siemens D5000 diffractometer with Cu K_α radiation operating at 30 kV and 40 mA and a scan range of 20–70° 2θ. N_2 adsorption–desorption isotherms were measured with a Micromeritics ASAP 2020 automatic adsorption instrument using nitrogen as the analysis gas. The data were analyzed with the Brunauer–Emmett–Teller (BET) equation to calculate the surface area. Scanning Transmission Electron Microscopy (STEM) measurements were carried out on JEM-2010F manufactured by JEOL, USA. A small amount of the catalyst sample was dispersed in isopropanol and sonicated for 10 min. A drop of the sample was then placed onto a carbon-coated copper grid (200 mesh, SPI supplies, USA). The grid supported sample was finally dried in an ultra-infrared lamp until isopropanol evaporated thoroughly. High angle annular dark field (HAADF) imaging was performed at 200 kV and extracting voltage of 4500 V. X-ray photoelectron spectroscopy (XPS) analysis was carried out with a monochromatic Al X-ray source fitted with a charge neutralization coil. Binding energies were referenced to C 1s peak at 285 eV. The vacuum level during the experiments was 10^{-7} Pa.

2.4 Antibacterial activity

The antibacterial analysis of normal Ag/TiO_2 and nano-Ag/TiO_2 particles was carried out by minimum inhibitory concentration (MIC) technique and the antibacterial effect of packaging with normal Ag/TiO_2 and nano-Ag/TiO_2 particles were tested against mould that isolated from aged rice. The packaging was produced using the method of Li Li.[21] In a typical process, 25 g of aged rice was placed in a stomacher bag containing 225 mL of 0.85% aseptic physiological saline and pummeled for 5 min. The homogenate was standardized to a concentration of at least 1×10^5 cell per mL using plate count. The Ag/TiO_2 particle was dispersed in sterile ultrapure water using ultrasonic vibration, and the suspension was serially diluted into 10, 1, 0.1, 0.01, 0.001 mg L^{-1}. The MIC was determined by spread plate method where 500 μL of antibacterial suspension and 200 μL of bacteria solution were poured and plated onto sterile Rose Bengal Agar (RBA) plate. The plates were then incubated at 28 °C for 48 ± 2 h and the distinct colonies were counted after that.

To test the antibacterial capacity of the two antibacterial packing, a modification of the International Standard ISO 22196:2007 was used. 1 mL mould suspension that prepared according the above method was daubed onto films. After two days, the films were washed by aseptic physiological saline and the antibacterial results were shown by the plate count.

Table 1 Preparation methods and Ag loadings of TiO_2 supported with different precursor

Samples[a]	Preparation method	Surface area ($m^2\ g^{-1}$)	Initial pH	Final pH	Uptake (μmol m^{-2})	Ag loading (wt%)
Ag/TiO_2	SEA	75.1	11.49	10.92	1.08	0.88
Ag/TiO_2-N	SEA	91.3	11.49	11.01	1.03	1.01

[a] BET surface area 79.3 $m^2\ g^{-1}$ for TiO_2 and 93.7 $m^2\ g^{-1}$ TiO_2-N.

3. Result and discussion

3.1 Preliminary equilibrium adsorption

Fig. 1a displays the pH shifts for $[Ag(NH_3)_2]^+$ adsorption experiments over TiO_2 and TiO_2-N. The pH shift curves after adsorption have similar trends as other oxides studied previous.[32] It is important to measure the optimum final pH required for maximum $[Ag(NH_3)_2]^+$ uptake on TiO_2 and TiO_2-N, which are shown in Fig. 1b. For both of different TiO_2 precursors, little $[Ag(NH_3)_2]^+$ is adsorbed below pH 9, but the adsorption increases rapidly with increasing pH, particularly between pH from 10 to 11.0. The adsorption decrease a little when pH reach 11.5, which is caused by the strong and competition adsorption of another cation at highest pH. The optimum pH final for TiO_2 and TiO_2-N are around 11, where the maximum uptakes are both around 1.1 μmol m^{-2}. The Ag loading of the samples prepared at the pH of maximum uptake, which corresponds to the optimal condition for SEA is 0.88 wt% and 1.01 wt% respectively (Table 1).

3.2 Characterization of nanoparticles

Fig. 2 shows STEM images of Ag/TiO_2-N and Ag/TiO_2 prepared with the SEA method. Fig. 2a displays the STEM micrograph where it can be observed TiO_2-N nanocrystals with particle sizes of 20–50 nm. Ag nanoparticles are observed as white spots on light grey TiO_2-N, and the Ag nanoparticles are generally spherical in shape.[38] The average particle size of Ag calculated from STEM images is quite small (1.8 nm), indicating that the SEA method could homogeneously deposit Ag particles over TiO_2-N surface (Fig. 2b). Fig. 2c and d show STEM image and the particle size distribution of Ag/TiO_2, which is limited to a narrow range as well, as shown by the values of standard deviation. It is worth noting that the optimal Ag uptake is found to be around 1 μmol m^{-2} onto both TiO_2 and TiO_2-N surface (Table 1). According to the BET method, the surface area of TiO_2 precursors lost little after deposition using SEA method. The oxide surface is strongly charged and the precursors deposited on individual adsorption sites at the pH of the strongest electrostatic attraction result in uniform dispersion of Ag nanoparticles with no Ag agglomeration. These results suggest that the synthesized nanocomposite is stable in nature.

The good Ag dispersion observed locally by STEM was confirmed at global scale using X-ray diffraction (XRD). Fig. 3 shows XRD patterns of TiO_2, TiO_2-N, Ag/TiO_2, Ag/TiO_2-N and metal Ag. A typical anatase phase TiO_2 crystal is observed from both commercial TiO_2 and nano-sized TiO_2-N. The mean crystalline size of TiO_2-N is evaluated to be around 23 nm based on Scherrer's equation from (101) peak.[39] It is agreed with the model TiO_2-N used as precursor. The power XRD pattern of Ag (Fig. 3e) exhibits cubic phase with peaks at 38.2°, 44.4°, 64.4° and 77.4° (JCPDS 03-0921). The power XRD pattern of Ag/TiO_2 shows the characteristic peaks corresponding to anatase TiO_2 phase. However, no characteristic peaks corresponding to Ag phase are observed, which confirms that the Ag particles are very small and highly dispersed on the TiO_2 support. It can be explicated that once the particle size is less than 3 nm, the characteristic peaks cannot be detected,[33] which is in agreement with the result of STEM. The XRD pattern of the Ag/TiO_2-N in Fig. 3d also shows that the Ag phase is well dispersed on support surface, since no peaks can be observed. This is also in agreement with the STEM result reported above. From XRD, it seems that using SEA method to prepare the Ag based antimicrobial agent can lead to very different formulations for the antibacterial active sites affecting antibacterial procedure.

The comparison of XPS spectra for Ag $3d_{3/2}$ and Ag $3d_{5/2}$ regions for samples supported with TiO_2 and TiO_2-N are provided in Fig. 4. As shown in the XPS, a small amount of Ag element is present. The Ag ($3d_{3/2}$) and Ag ($3d_{5/2}$) peaks are found at binding energy of 368.4 and 374.4 eV, respectively, in both of the two samples. In particular, the splitting of the 3d doublet of Ag is 6.0 eV, indicating formation of metallic silver nanoparticles[40] on surface of the Ag/TiO_2-N. To further study the chemical state of the silver atoms accumulated on the surface, a detailed deconvolution of Ag (3d) peak was also performed. There are three components after deconvolution according to the binding energy of Ag core level for Ag (368.4 eV), Ag_2O (367.6 eV) and AgO (367.05 eV). The peak is deconvoluted into two Gaussian components with identical full width at half maximum (FWHM) after a Shirley back-ground subtraction. Based on the deconvolution analysis, it is found that most of the silver atoms accumulated on the surface are in the Ag (metallic) state, while only little silver atoms are in Ag^+ chemical states and no silver atoms are in Ag^{2+}. The ratio of Ag^+ on the TiO_2-N is a little more than that on TiO_2, however, no obvious difference was found between the samples using

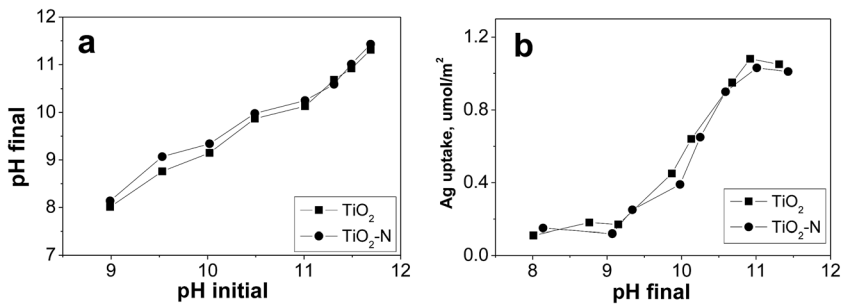

Fig. 1 (a) pH shift with pure oxides-control experiment; $[Ag(NH_3)_2]^+$ solution pH shifts for TiO_2 (~200 ppm $[Ag(NH_3)_2]^+$, 500 m^2 L^{-1}) (b) Ag uptake on TiO_2 *versus* pH.

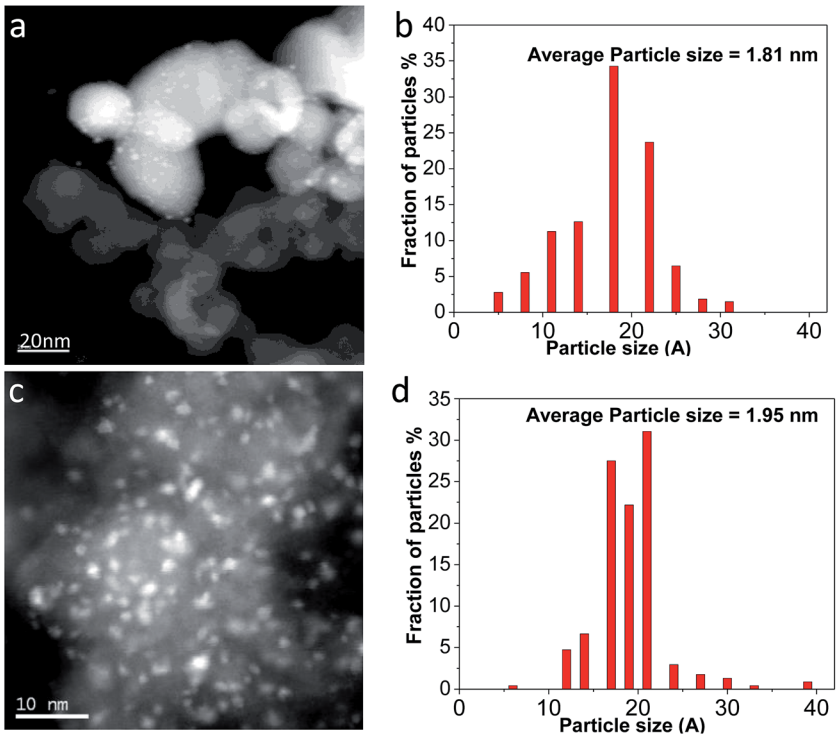

Fig. 2 STEM image of (a) Ag/TiO_2-N, (c) Ag/TiO_2 and (b) and (d) its particle size distribution.

different support. It is explicated that deposition $[Ag(NH_3)_2]^+$ on TiO_2 using SEA after UV irradiation results in different Ag^0 and Ag^+ composition and while metallic Ag plays a crucial role in electron transfer from TiO_2.

3.3 Antibacterial activity

The antibacterial activity of the as-prepared samples and minimum inhibitory concentrations were investigated by measuring the growth inhibition of the mould that isolated from aged rice on Bengal medium solid agar plates. Fig. 5 shows

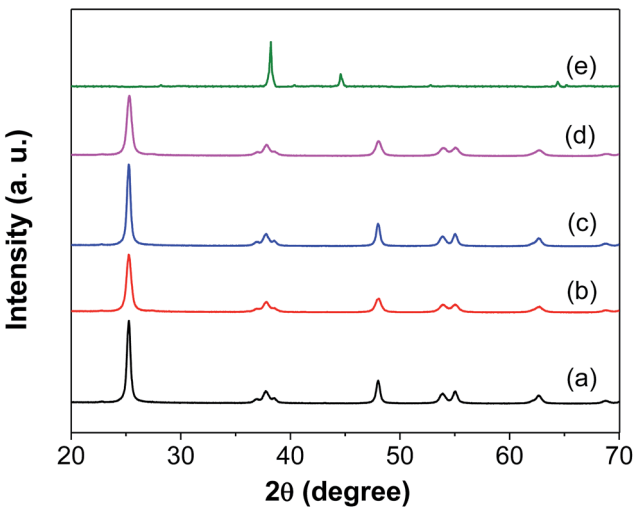

Fig. 3 XRD patterns of (a) TiO_2, (b) TiO_2-N, (c) Ag/TiO_2, (d) Ag/TiO_2-N, (e) Ag.

that Ag/TiO_2 particles could inhibit the mould growth and have an increase antibacterial effect with increasing the Ag/TiO_2 concentration. When the concentration is 1 mg L^{-1}, the inhibition rate of normal-Ag/TiO_2 and Ag/TiO_2-N is more than 96% and has no significant difference between each other. With higher concentration of particles (10 mg L^{-1}), there is little change of inhibitory effect under the test conditions. So, the minimum inhibitory concentration of 1 mg L^{-1} is the optimal inhibitory concentration in mold growth. Silver has a broad spectrum of antibacterial activities, especially for the nanosized silver. Nanostructured antibacterial have high surface area-to-volume ratio compared with higher scale counterparts. The silver adsorbed onto TiO_2 is nanosized with a narrow size. The normal-Ag/TiO_2 and Ag/TiO_2-N could release silver ions a long term and generate chemical species reactive to oxygen, form complexes with sulfur, nitrogen and oxygen, which leading to the cell death. Fig. 6a–c show the antibacterial activity of the packaging with Ag/TiO_2 particle, packaging with Ag/TiO_2-N particle and the normal packaging. The antibacterial activity of two antibacterial packaging can inhibit the mould growth and the total plate count is scare compared with the blank control that normal packaging had not added the antimicrobial agent. It is indicated that silver deposition onto different supports shows almost the same antibacterial performance. The packaging with antibacterial property can be used as a functional material in fruits and vegetables logistics. As we known, most fresh food should been packed for facilitate sales and resistance of the environmental pollution. The antibacterial packaging is efficient for retarding the changes of qualities of food and extend the shelf life. The higher inhibitory of Ag/TiO_2 against

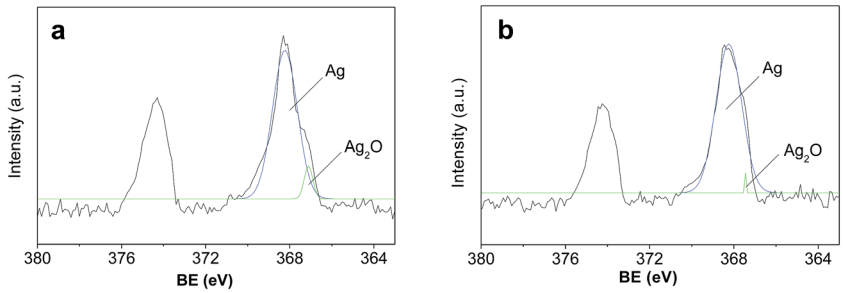

Fig. 4 XPS spectra of (a) Ag/TiO_2-N, and (b) Ag/TiO_2.

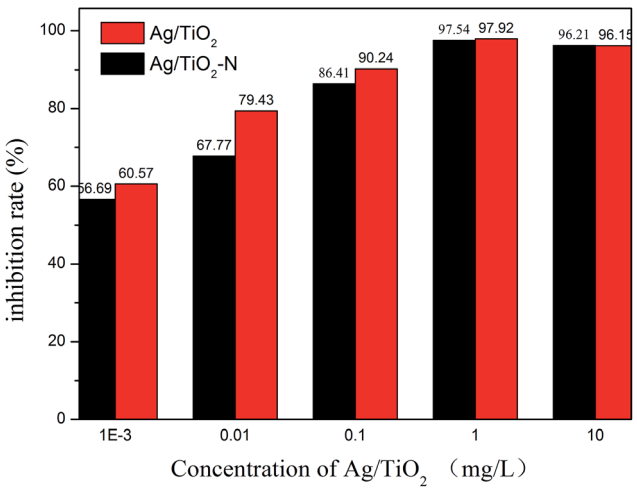

Fig. 5 The antibacterial rate of different concentrations of Ag/TiO_2.

mould in low concentration may be attributed to the uniformly distributed silver on TiO_2 and the size of Ag. The inhibitory effect of Ag/TiO_2 particles is related to their shape, state of aggregation and size.[41] Silver nanoparticles with a size of about 2 nm are well known for their antibacterial properties because silver ions could migrate and attach to the cell membrane, leading to changes of cell structure, membrane permeability and cellular enzymes, ultimately resulting in the bacteria death.[42–44] Ag/TiO_2 nanoparticles prepared by SEA method using a strong electrostatic can keep stable releasing of silver with a long term and improve the utilization efficiency of silver and make the silver particles distribute on TiO_2 uniformly, thus improving the inhibitory efficiency in attacking and destructing bacterial cell membranes.

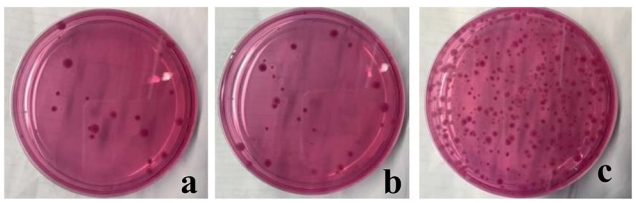

Fig. 6 The antibacterial activity of packaging with Ag/TiO_2 (a), Ag/TiO_2-N (b) and normal packaging (c) to mould.

4. Conclusion

Ag/TiO_2 and Ag/TiO_2 nanopowder were synthesized by SEA method and well-dispersed Ag particles on TiO_2 were obtained during the preparation process. Owing to the strong electrostatic adsorption that exists between the Ag precursor and TiO_2, the intrinsic principles for deposition and the strong electrostatic interaction using SEA method prevented sintering and agglomeration of particles during UV reduction, which led to the formation of very uniform and small Ag particles on TiO_2. Both of the Ag based antibacterial samples and packaging were proven to be great inhibitory efficiency of mould growth in attacking and destructing bacterial cell membranes. Finally, it is suggested that the use of SEA in the preparation of metal supported materials is a viable way where intimate contact between different metals is desired.

Acknowledgements

This research was supported by the National key research and development program of China (2016YFD0400901), the National Natural Science Foundation of China (Grant No. 31571901), the Natural Science Foundation of Jiangsu Province (BK20141486), Agricultural independent innovation fund of Jiangsu Province (CX(16)1062), Development Program of Jiangsu Province (BK2016386) and the Priority Academic Program Development of Jiangsu Higher Education Institutions.

References

1 W. Hou and S. B. Cronin, *Adv. Funct. Mater.*, 2013, **23**, 1612–1619.
2 T. Møretrø, G. S. Høiby-Pettersen, C. K. Halvorsen and S. Langsrud, *Food Control*, 2012, **28**, 118–121.
3 K. B. Holt and A. J. Bard, *Biochemistry*, 2005, **44**, 13214–13223.
4 K. S. Abhijith, R. Sharma, R. Ranjan and M. S. Thakur, *Photochem. Photobiol. Sci.*, 2014, **13**, 986–991.
5 Y. Matsumura, K. Yoshikata, S. Kunisaki and T. Tsuchido, *Appl. Environ. Microbiol.*, 2003, **69**(7), 4278–4281.
6 V. Kumar, M. S. Basu and T. P. Rajendran, *Crop Prot.*, 2008, **27**, 891–905.

7 Y. Lu and W. Chen, *1D Pd-Based Nanomaterials as Efficient Electrocatalysts for Fuel Cells*, 2014, pp. 321–357.
8 J. E. Millstone, S. J. Hurst, G. S. Métraux, J. I. Cutler and C. A. Mirkin, *Small*, 2009, **5**, 646–664.
9 Y. Yin and A. P. Alivisatos, *Nature*, 2005, **437**, 664–670.
10 T. K. Sau and A. L. Rogach, *Adv. Mater.*, 2010, **22**, 1781–1804.
11 N. Z. And and G. D. Stucky, *J. Am. Chem. Soc.*, 2006, **128**, 14278–14280.
12 Z. Deng, M. Chen and L. Wu, *J. Phys. Chem. C*, 2007, **111**, 11692–11698.
13 Z. Li, L. Fan, T. Zhang and K. Li, *J. Hazard. Mater.*, 2011, **187**, 466–472.
14 L. Liu, J. Liu, Y. Wang, X. Yan and D. D. Sun, *New J. Chem.*, 2011, **7**, 1418–1423.
15 A. L. Motlagh, S. Bastani and M. M. Hashemi, *Prog. Org. Coat.*, 2014, **77**, 502–511.
16 D. Tang, R. Yuan and Y. Chai, *J. Phys. Chem. B*, 2006, **110**, 11640–11646.
17 M. R. Hoffmann, W. Choi and D. W. Bahnemann, *Chem. Rev.*, 1995, **95**, 69–96.
18 D. A. P. D. Abreu, J. M. Cruz, I. Angulo and P. P. Losada, *Packag. Technol. Sci.*, 2010, **23**, 59–68.
19 D. L. Fang, W. J. Yang, B. M. Kimatu, A. M. Mariga, L. Y. Zhao, X. X. An and Q. H. Hu, *Innovative Food Sci. Emerging Technol.*, 2015, **33**, 489–497.
20 F. M. Yang, H. M. Li, F. Li, Z. H. Xin, L. Y. Zhao, Y. H. Zheng and Q. H. Hu, *Food Sci.*, 2010, **75**(3), C236–C240.
21 L. Li, C. J. Zhao, Y. D. Zhang, J. F. Yao, W. J. Yang, Q. H. Hu, C. L. Wang and C. J. Cao, *Food Chem.*, 2017, **215**, 477–482.
22 Z. Zheng, B. B. Huang, X. Y. Qin, X. Y. Zhang and Y. Dai, *J. Mater. Chem.*, 2011, **21**, 9079–9087.
23 H. Zhang, X. Li and G. Chen, *J. Mater. Chem.*, 2009, **19**, 8223–8231.
24 S. F. Chen, J. P. Li, K. Qian, W. P. Xu, Y. Lu, W. X. Huang and S. H. Yu, *Nano Res.*, 2010, **3**, 244–255.
25 H. Zhang and G. Chen, *Environ. Sci. Technol.*, 2009, **43**, 2905–2910.
26 R. Liu, P. Wang, X. Wang, H. Yu and J. Yu, *J. Phys. Chem. C*, 2012, **116**, 17721–17728.
27 S. K. Gogoi, P. Gopinath, A. Paul, A. Ramesh, S. S. Ghosh and A. Chattopadhyay, *Langmuir*, 2006, **22**, 9322–9328.
28 X. H. Xu, W. J. Brownlow, S. V. Kyriacoou, Q. Wan and J. J. Viola, *Biochemistry*, 2004, **43**, 10400–10413.
29 F. X. Zhang, N. J. Guan, Y. Z. Li, X. Zhang and J. X. Chen, *Langmuir*, 2003, **19**, 8230–8234.
30 I. Bano, R. V. Kumar and A. Hameed, *Ionics*, 2012, **18**, 307–313.
31 S. C. Chan and M. A. Barteau, *Langmuir*, 2005, **21**, 5588–5595.
32 J. R. Regalbuto, A. Navada, S. Shadid, M. L. Bricker and Q. Chen, *J. Catal.*, 1999, **184**, 335–348.
33 C. Cao, G. Yang, L. Dubau, F. Maillard, S. D. Lambert, J. P. Pirard and N. Job, *Appl. Catal., B*, 2014, **150–151**, 101–106.
34 L. D. Souza, L. Jiao, J. R. Regalbuto, J. T. Miller and A. J. Kropf, *J. Catal.*, 2007, **248**, 165–174.
35 C. J. Cao, G. Yang, W. Song, X. R. Ju, Q. H. Hu and J. F. Yao, *J. Power Sources*, 2014, **272**, 1030–1036.
36 J. P. Brunelle, *Pure Appl. Chem.*, 1978, **50**, 1211–1229.
37 J. Park and J. R. Regalbuto, *J. Colloid Interface Sci.*, 1995, **175**, 239–252.
38 A. Zielińska, E. Kowalska, J. W. Sobczak, L. Lacka, M. Gazda and B. Ohtani, *Sep. Purif. Technol.*, 2010, **72**, 309–318.
39 K. Kaji, *Fiber*, 1975, **31**, 204–214.
40 R. Sanjines, *J. Appl. Phys.*, 1994, **75**, 2945–2951.
41 A. Klančnik, S. Piskernik, B. Jeršek and S. S. Možina, *J. Microbiol. Methods*, 2010, **81**, 121–126.
42 O. Yamamoto, M. Komatsu, J. Sawai and Z. Nakagawa, *J. Mater. Sci.: Mater. Med.*, 2004, **15**, 847–851.
43 G. Colon and B. C. W. J. Webster, *J. Biomed. Mater. Res., Part A*, 2006, **78**, 595–604.
44 M. Rai, A. Yadav and A. Gade, *Biotechnol. Adv.*, 2010, **27**, 76–83.

